Electronic Supplementary Material (ESI) for Journal of Materials Chemistry C.

Low resistivity HfN_x grown by plasma-assisted ALD with external rf substrate biasing

Saurabh Karwal[*†], Marcel A. Verheijen[†‡], Benjamin L. Williams[†], Tahsin Faraz[†], Wilhelmus M.M. Kessels[†ζ] and Mariadriana Creatore[†ζ]

[†]Department of Applied Physics, University of Technology Eindhoven, 5600MB, P.O. Box 513, Eindhoven, Netherlands

[‡]Philips Innovation labs, High Tech Campus 11, 5656 AE Eindhoven, The Netherlands

[ζ]Solliance, High Tech Campus 21, 5656AE, Eindhoven, Netherlands

HfN_x ALD process

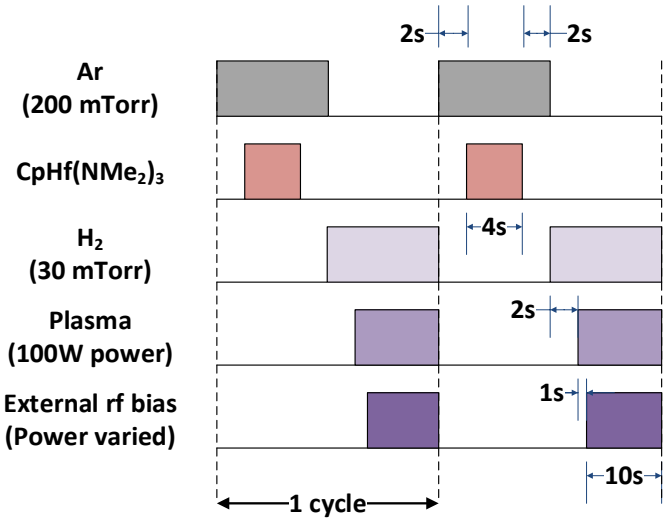

Figure S1. Time sequence for the complete ALD cycles of HfN_x using $CpHf(NMe_2)_3$ and H_2 plasma depicting the application of an external rf substrate bias during the H_2 plasma step. A plasma stabilization time of 1s was used and can be neglected. Time intervals are not drawn to scale.

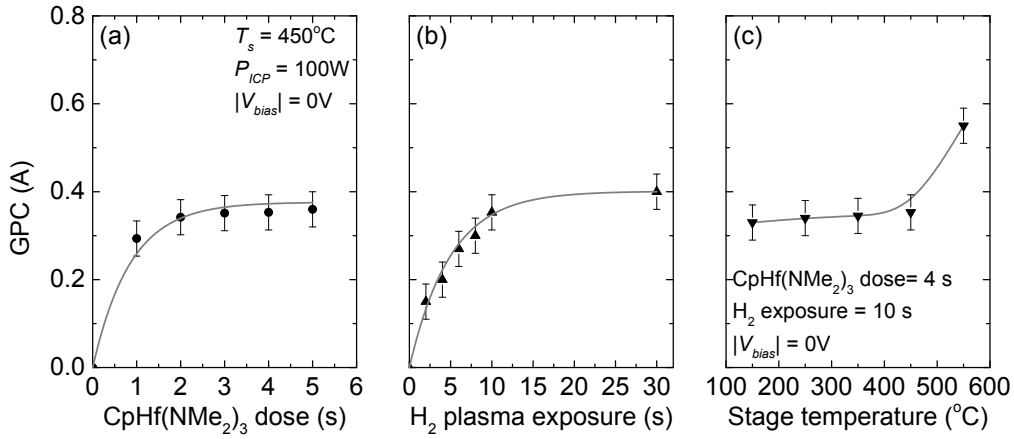

Figure S2. Growth per cycle (GPC) (Å) for HfN_x films prepared at $|V_{bias}|$ = 0V as a function of (a) $CpHf(NMe_2)_3$ dose time and (b) H_2 plasma exposure time. The $CpHf(NMe_2)_3$ dose, H_2 plasma exposure and purge times under saturation conditions were 4 s, 10 s and 2 s respectively. (c) GPC(Å) for the HfN_x films prepared under saturation conditions as a function of the stage temperature showing an abrupt increase above 450°C. Lines serve as a guide to the eye.

Figure S3a shows a linear thickness increase with number of ALD cycles for HfN_x films prepared at various values of $|V_{bias}|$. Furthermore, the ALD process was found to saturate using a $CpHf(NMe_2)_3$ dose time of 4 s at all values of $|V_{bias}|$ investigated (Figure S3b). Therefore, the application of external rf substrate bias does not affect the self-saturation behavior of the ALD process. The HfN_x films were also prepared at $|V_{bias}|$ = 0V and at $|V_{bias}|$ = 187V on 8-inch Si wafers and the thickness non-uniformity was evaluated (Figure S3c). The thickness non-uniformity was deduced by taking the ratio between standard deviation and average film thickness (1-sigma). A similar thickness non-uniformity of 9.1% and 7.8% was obtained for the HfN_x films prepared with grounded electrode and at $|V_{bias}|$ = 187V respectively.

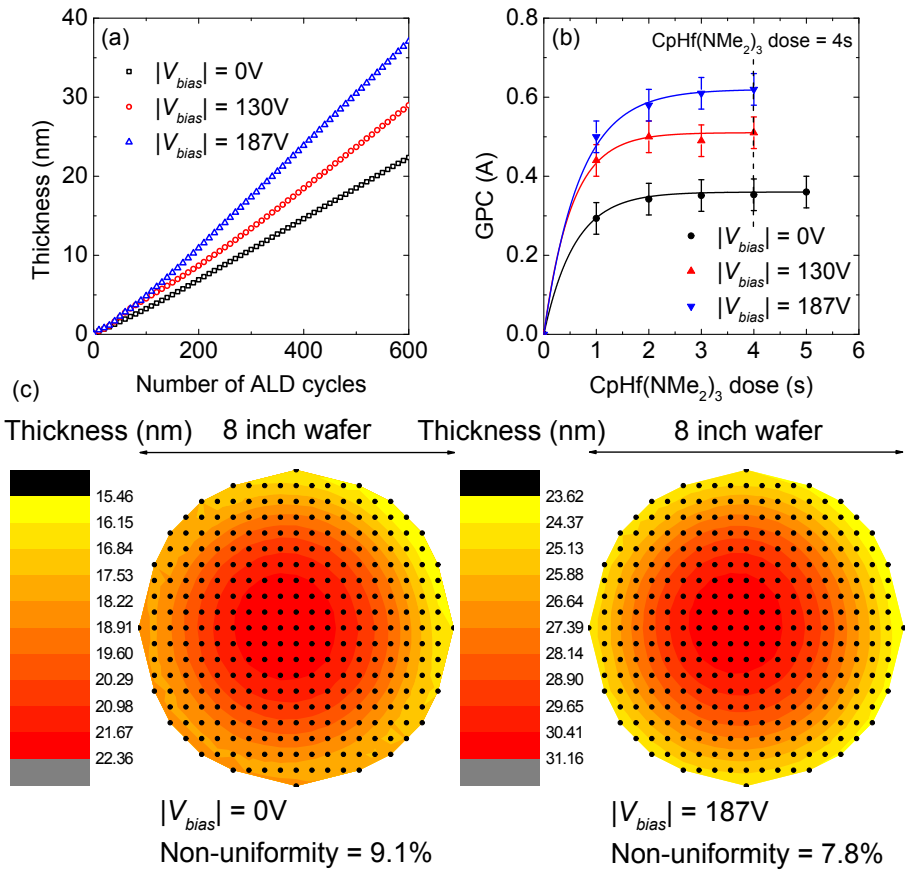

Figure S3. (a) HfN_x film thickness as a function of number of ALD cycles prepared for various values of $|V_{bias}|$; (b) GPC(Å) as a function of $CpHf(NMe_2)_3$ dose time for HfN_x films prepared at various values of $|V_{bias}|$; (c) thickness uniformity maps on 8-inch Si wafer for HfN_x films prepared with grounded electrode ($|V_{bias}|$ = 0V) and at $|V_{bias}|$ = 187V showing a similar thickness non-uniformity in both cases. The black points on the wafer are the actual measurement points with 5 mm edge exclusion.

Modeling of HfN_x dielectric functions using spectroscopic ellipsometry

The dielectric functions can be modelled using one Drude and two Lorentz oscillators:

$$\varepsilon(E) = \varepsilon_1(E) + i\varepsilon_2(E) = \varepsilon_\infty - \overbrace{\frac{E_p^2}{E^2 - i\Gamma_D E}}^{Drude} + \sum_{j=1}^{2} \overbrace{\frac{S_j E_{0j}^2}{E_{0j}^2 - E_j^2 + iE_j\Gamma_j}}^{Lorentz} \quad (1)$$

where, ε_∞ represents transitions at higher energy which are not accounted in Lorentz oscillators, E_p is plasma energy and Γ_D is the damping factor for Drude oscillator. The Lorentz oscillators are centered at E_o which corresponds to the resonance frequency, while S indicates the strength of the oscillators and Γ is the damping factor for the Lorentz oscillators.

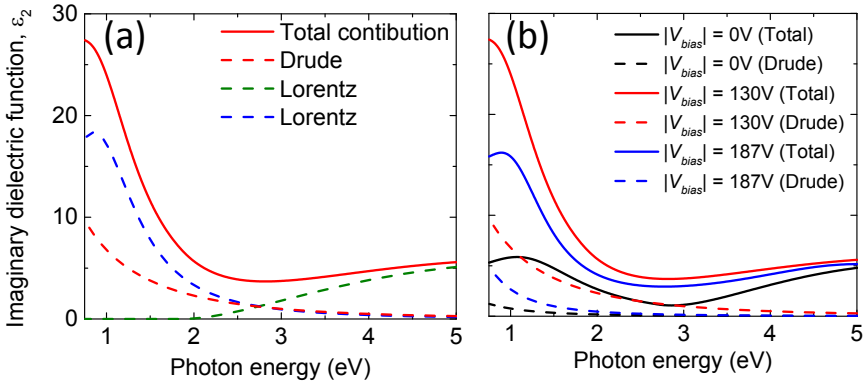

Figure S4. Imaginary dielectric function ε_2 for the δ-HfN_x films prepared at (a) $|V_{bias}|$ = 130V obtained *via* fitting of the ellipsometry data with parameterization including one Drude and two Lorentz oscillators and (b) various values $|V_{bias}|$. The individual Drude oscillators for the films are also given revealing an increase in Drude absorption by applying an external rf substrate bias.

Table S1. SE fitting parameter values for one Drude and two Lorentz oscillators for the δ-HfN film prepared at $|V_{bias}|$ = 130V.

$\|V_{bias}\|$ (V)		130
ε_∞		4.15
E_p (eV)		1.7
Lorentz oscillator 1	S (eV)	19.4
	Γ (eV)	1.2
	E_o (eV)	1.1
Lorentz oscillator 2	S (eV)	5.4
	Γ (eV)	4.3
	E_o (eV)	5.7

Knoops *et al.* described that the insights into grain boundary scattering can be gained by probing opto-electronic properties using SE.[1] In Figure S4, the imaginary part of the dielectric function ε_2 and the corresponding Drude absorption for the HfN_x films grown at various values of $|V_{bias}|$ are presented. An optical resistivity (ρ_{op}) of $(5.9\pm0.1)\cdot10^{-3}$ Ωcm was deduced from the magnitude of Drude absorption for the HfN_x film grown with grounded electrode ($|V_{bias}|$ = 0V). An increase in $|V_{bias}|$ to 130V led to an increase in the magnitude of Drude absorption, signifying an increase in the in-grain conduction electron density. An ρ_{op} of $(9.0\pm0.2)\cdot10^{-4}$ Ωcm was deduced for the HfN_x film grown at $|V_{bias}|$ = 130V. A further increase in the $|V_{bias}|$ to 187V led to a decrease in the magnitude of Drude absorption and an increase in ρ_{op} to $(1.7\pm0.1)\cdot10^{-3}$ Ωcm. In addition, the

interaction distance (d_{int}) of the incident light with the HfN_x films was calculated using the HfN effective mass of 0.88,[2] the fermi velocity $\left(v_e = \hbar(3\pi^2 N)^{1/3} / m^*\right)$ and a photon energy of 0.75 eV (lower limit of SE) in the same manner as described by Knoops et al.[1] An d_{int} of 2.3 nm, 3.3 nm and 2.9 nm were deduced for HfN_x films grown at $|V_{bias}|$ of 0V, 130V and 187V respectively. In-view of the small interaction distance as compared to the lateral grain size of ~20-25 nm of the HfN_x films (as will be explained in microstructural characterization section), it is plausible to use the difference between electrical and optical resistivity in order to judge the extent of scattering at the grain boundaries as a function of $|V_{bias}|$.

Chemical composition analyses of HfN_x films using X-ray photoelectron spectroscopy

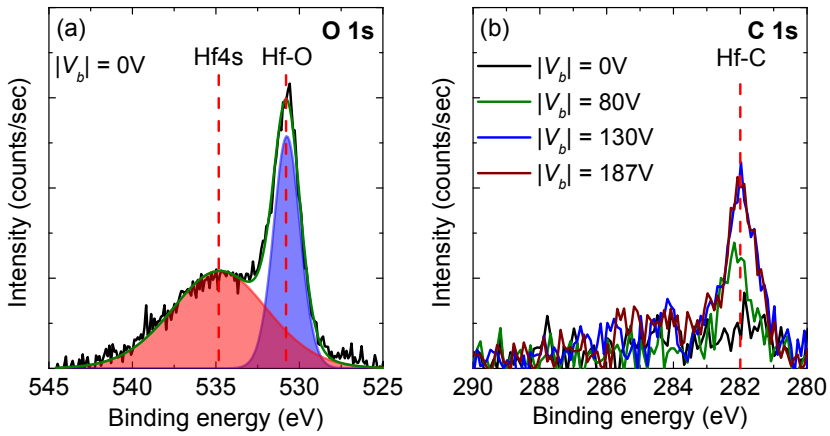

Figure S5. (a) De-convoluted O 1s XPS spectrum for HfN_x film prepared at $|V_{bias}|$ = 0V showing the presence of Hf-O bonds and (b) C 1s XPS spectra for HfN_x films prepared at various values of $|V_{bias}|$ showing an increase in the peak intensity of Hf-C bonds with an increase in $|V_{bias}|$.

Table S2. Corresponding peak assignment, binding energies and full width half maximum for the Hf, N, O and C spectral lines used to deconvolute the peaks, measured by XPS.

Spectral line	Peak designation	Binding energy (eV)	FWHM (eV)	Reference
Hf $4f_{7/2}$	Hf^{4+}	16.0	1.6	3,4
Hf $4f_{7/2}$	Hf^{3+}	14.9	1.6	5
N 1s	$Hf^{3+}N$	397.5	1.5	6
N 1s	$Hf^{4+}N$	396.5	1.6	7

O 1s	HfO_x	530.8	1.9	[8]
C 1s	HfC_x	282	1.2	[9]

Variation of GPC (Å) with GPC (Hf atoms nm^{-2})

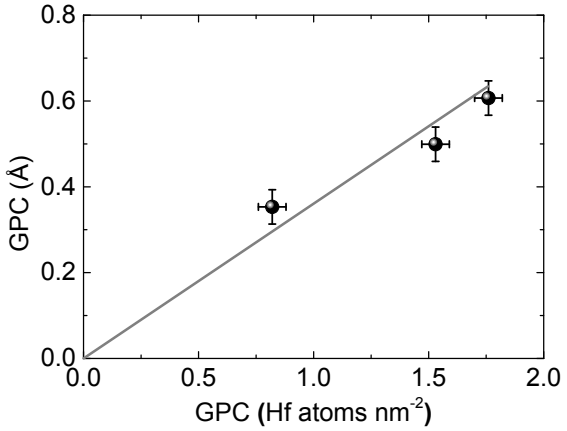

Figure S6. GPC in terms of thickness as a function of GPC in terms of Hf atoms deposited per nm^2 illustrating a proportional dependence.

GIXRD patterns for HfN_x films as a function of $|V_{bias}|$

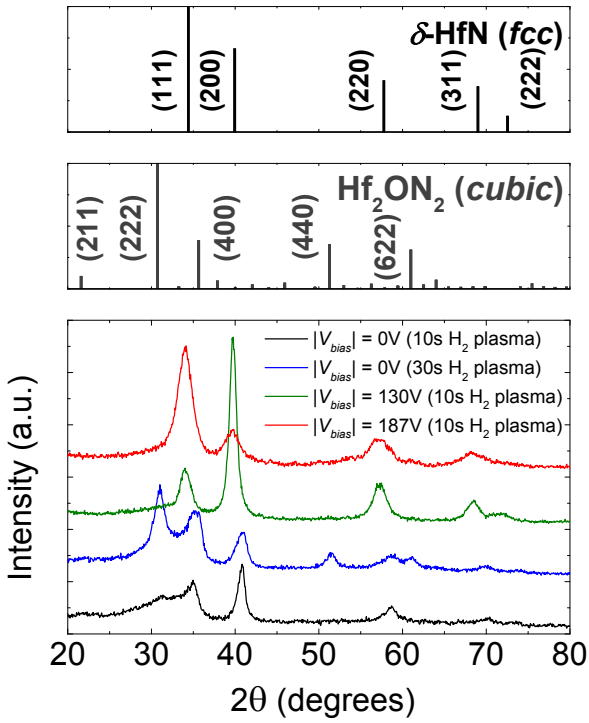

Figure S7. Grazing incidence X-ray diffractograms for ~75 nm thick HfN_x films prepared at various values of $|V_{bias}|$ referenced with powder *fcc* δ-HfN and *cubic* Hf_2ON_2 XRD patterns.

HAADF-STEM images for HfN_x films during nucleation phase

The development of microstructure was studied during the nucleation phase of film growth by preparing ~15 nm of HfN_x films on Si_3N_4 TEM windows that are coated with ~5 nm ALD SiO_2. Figure S8 shows the HAADF-STEM images of the HfN_x layers deposited at various values of $|V_{bias}|$. The HfN_x film grown at $|V_{bias}|$ = 130V exhibits a lateral grain size of 7.5±2.0 nm whereas the film grown at $|V_{bias}|$ = 187V was found to be nanocrystalline in nature. In addition, the selected area electron diffraction patterns (SAED) were acquired from 1.3 μm diameter areas for the corresponding HfN_x films (insets in Figure S8). Interestingly, no significant difference in crystallographic texture was observed in the nucleation layer for both the HfN_x films. However, the HfN_x film grown at $|V_{bias}|$ = 130V exhibits discontinuous diffraction rings signifying the formation of relatively *large* crystallites whereas a more continuous diffraction pattern was

obtained for the HfN_x film grown at $|V_{bias}|$ = 187V. This result implies that at $|V_{bias}|$ = 187V, relatively *small* lateral crystallites are formed.

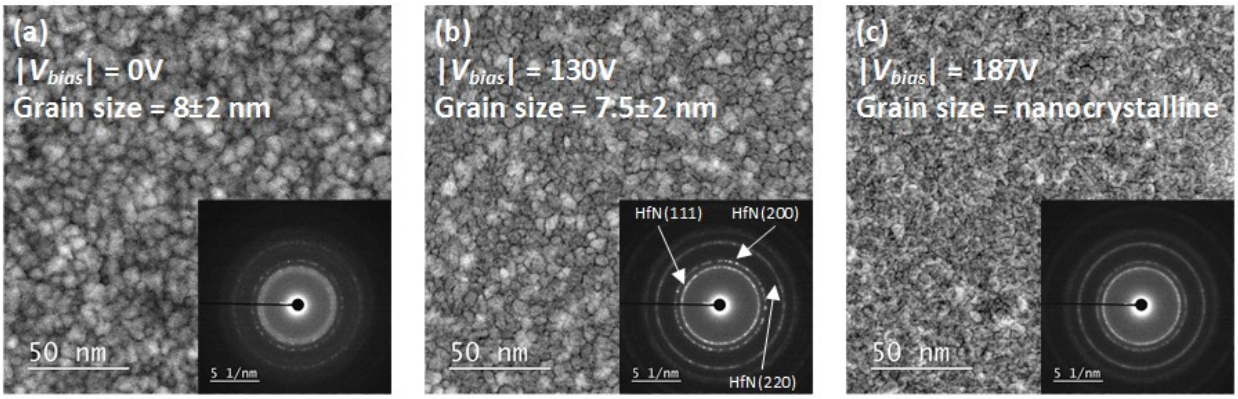

Figure S8. Top-view high-angle annular dark-field scanning transmission electron microscope (HAADF-STEM) images for ~15 nm thick HfN_x films prepared (a) $|V_{bias}|$ = 0V (b) $|V_{bias}|$ = 130V and (c) $|V_{bias}|$ = 187V. Inset depicts the corresponding selected area electron diffraction (SAED) patterns.

References

1 Knoops, H. C. M. *et al.* Optical modeling of plasma-deposited ZnO films: Electron scattering at different length scales. *Journal of Vacuum Science & Technology A* **33**, 021509, doi:doi:http://dx.doi.org/10.1116/1.4905086 (2015).

2 Strømme, M., Karmhag, R. & Ribbing, C. G. Optical constants of sputtered hafnium nitride films. Intra- and interband contributions. *Optical Materials* **4**, 629-639, doi:http://dx.doi.org/10.1016/0925-3467(95)00006-2 (1995).

3 Kang, C. S. *et al.* Bonding states and electrical properties of ultrathin HfOxN y gate dielectrics. *Appl Phys Lett* **81**, 2593-2595, doi:10.1063/1.1510155 (2002).

4 Arranz, A. Synthesis of hafnium nitride films by 0.5-5 keV nitrogen implantation of metallic Hf: An X-ray photoelectron spectroscopy and factor analysis study. *Surf Sci* **563**, 1-12, doi:10.1016/j.susc.2004.06.162 (2004).

5 Wang, W., Nabatame, T. & Shimogaki, Y. Preparation of conductive HfN by post rapid thermal annealing-assisted MOCVD and its application to metal gate electrode. *Microelectronic Engineering* **85**, 320-326, doi:http://dx.doi.org/10.1016/j.mee.2007.07.003 (2008).

6 Shinkai, S. & Sasaki, K. Influence of sputtering parameters on the formation process of high-quality and low-resistivity HfN thin film. *Jpn J Appl Phys Part 1 Regul Pap Short Note Rev Pap* **38**, 2097-2102 (1999).

7 Wang, W., Nabatame, T. & Shimogaki, Y. Interface structure of HfNx/SiO2 stack grown by MOCVD using TDEAHf precursor. *Surf Sci* **588**, 108-116, doi:10.1016/j.susc.2005.05.035 (2005).

8 Kirsch, P. D., Kang, C. S., Lozano, J., Lee, J. C. & Ekerdt, J. G. Electrical and spectroscopic comparison of HfO 2/Si interfaces on nitrided and un-nitrided Si(100). *J Appl Phys* **91**, 4353-4363, doi:10.1063/1.1455155 (2002).

9 Jang, J. H. *et al.* Role of Carbon on Resistivity and Structure of Hf Cx Ny Films Grown by Low Temperature MOCVD. *J Electrochem Soc* **156**, H76-H79, doi:10.1149/1.3021038 (2009).